A computationally effective 3D Boundary Element Method for polycrystalline micromechanics

V. Gulizzi[1,a], I. Benedetti[1,b]

[1] Dipartimento di Ingegneria Civile, Ambientale, Aerospaziale e dei materiali,

Università degli Studi di Palermo, Viale delle Scienze, Edificio 8, 90128, Palermo, Italy

[a] vincenzo.gulizzi@unipa.it, [b] ivano.benedetti@unipa.it

Keywords: Polycrystalline materials; Micromechanics; Computational Homogenization; Microcracking; Representative Volume Element.

Abstract. An effective computational framework for homogenization and microcracking analysis of polycrystalline RVEs is presented. The method is based on a recently developed grain-boundary formulation for polycrystalline materials and several enhancements over the original technique are introduced to reduce the computational effort needed to model three-dimensional polycrystalline aggregates, which is highly desirable, especially in a multiscale perspective. First, a regularization scheme is used to remove *pathological* entities, usually responsible for unduly large mesh refinements, from Voronoi polycrystalline morphologies. Second, an improved meshing strategy is used, with an aim towards meshing robustness, a requirement often challenged by the inherent high statistical variability of Voronoi tessellations. Additionally, for homogenization purposes, the use of periodic *non-prismatic* polycrystalline RVEs is proposed as an alternative to the classical *prismatic* RVEs, generally employed in the literature. The proposed overall scheme promotes a remarkable reduction in the number of DoFs of the problem in hand, and thus outstanding savings in terms of computational time and memory storage. Furthermore, the smoother meshing strategy, combined with a Newton-Raphson method, enhances the convergence of the microcracking algorithm.

Introduction.

Natural as well as engineered materials are generally heterogeneous at a certain scale [1]. It is today recognised that the material microstructure strongly influences its macroscopic behaviour, at the application scale. As a consequence, accurate modelling of the microstructure is of relevant engineering interest.

Polycrystalline materials are aggregates of randomly oriented crystals characterized by their anisotropy, grain morphology and spatial distribution, and by the physical and chemical properties of the inter-granular interfaces. Polycrystalline structures are found at the micrometre scale in metals, alloys, and ceramics, which are widely employed in engineering applications. Although the direct simulation of a macro component involving the microscale details throughout the whole domain is practically unfeasible, due to the enormous number of heterogeneous micro-constituents, a clear distinction can be made between the two scales (i.e. the macro- and the micro-scale). As a consequence, *multiscale* techniques able to exchange information between the two scales represent an effective approach for such problems.

Multiscale modelling is based on the concept of Representative Volume Element (RVE). For polycrystalline materials, an RVE can be defined as a micro-sample containing a number of grains sufficient to reproduce, in their aggregate behaviour, the statistical features of the macro-material, but small enough to be considered as an infinitesimal point within the macro-continuum. Polycrystalline RVEs have been studied using both the finite element (FEM) [2,3] and boundary element (BEM) [4,5] methods [6].

However, even in a multiscale framework, the need to represent with sufficient accuracy the microstructural features, at the grain scale, typically leads to extremely large systems of equations [7]. Although modern High Performance Computing (HPC) has enormously favoured a general advancement in the treatment of such large scale problems, the ultimate goal of effective *multiscale modelling*, within a *computational homogenization* framework, is still hindered by the computational effort required to solve simultaneously many RVEs nested within the macroscale. This originates a strong interest in reducing, both in terms of storage and time, the computational effort associated with the single RVE computations.

In this work, a computationally effective boundary element framework for 3D polycrystalline micromechanics is presented. First, Voronoi tessellations, usually representing the crystalline micro-morphologies, are *regularized* using the technique proposed by Quey et Al. [8], with the aim to avoid the presence of small geometrical entities (edges and faces) usually inducing expensive mesh refinements.

Second, a general and robust *meshing strategy* is introduced in the grain boundary formulation developed in Ref. [4], to conjugate the effectiveness and simplicity of the grain boundary formulation with the need of reducing the total count of DoFs, also allowing a smoother representation of the intergranular fields with respect to the basic discontinuous scheme [4]. Additionally, a *non-prismatic* representation of the periodic RVE is proposed and adopted for homogenization purposes, avoiding some pathologies usually induced by common strategies adopted for generating periodic prismatic RVEs. The numerical tests show how the above enhancements remarkably reduce the computational effort in terms of both memory storage and solution time of the polycrystalline aggregate problem, thus paving the way towards effective multiscale modelling.

Grain boundary formulation.

The polycrystalline aggregate is modelled using a multi-domain boundary integral formulation [4,5], which leads to the following system of equations for a generic grain *g*

$$\boldsymbol{A}^g \boldsymbol{X}^g = \boldsymbol{C}^g \boldsymbol{Y}^g \tag{1}$$

where $\boldsymbol{X}^g$ collects the unknown values of grain-boundary displacements and tractions, $\boldsymbol{Y}^g$ collects prescribed values of boundary displacements and tractions, and $\boldsymbol{A}^g$ and $\boldsymbol{C}^g$ contains combinations of columns of the matrices stemming from the integration of the 3D anisotropic fundamental solutions [9]. Eq.(1) is written for each grain of the aggregate; enforcing suitable intergranular conditions then retrieves the integrity of the aggregate leading to the following system

$$\begin{bmatrix} \boldsymbol{A}\,\boldsymbol{X} \\ \boldsymbol{\Psi}(\boldsymbol{X}) \\ \boldsymbol{\Phi}(\boldsymbol{X}) \end{bmatrix} = \begin{Bmatrix} \boldsymbol{C}\,\boldsymbol{Y}(\lambda) \\ \boldsymbol{0} \\ \boldsymbol{0} \end{Bmatrix} \tag{2}$$

where $\boldsymbol{X} = \left\{ \boldsymbol{X}_1 \cdots \boldsymbol{X}_{N_g} \right\}$, $\boldsymbol{Y} = \left\{ \boldsymbol{Y}_1 \cdots \boldsymbol{Y}_{N_g} \right\}$ and the matrices $\boldsymbol{A}$ and $\boldsymbol{C}$ contain suitable combination of the matrices $\boldsymbol{A}^g$ and $\boldsymbol{C}^g$, $g = 1,...,N_g$ being N_g the number of grains. $\boldsymbol{\Psi}(\boldsymbol{X}) = \boldsymbol{0}$ and $\boldsymbol{\Phi}(\boldsymbol{X}) = \boldsymbol{0}$ implement the Interface Conditions (ICs), which in general can be function of the intergranular displacements and tractions fields. In particular, $\boldsymbol{\Psi}(\boldsymbol{X}) = \boldsymbol{0}$ represent either continuity, cohesive or frictional contact laws depending on the state of the interface [5]. $\boldsymbol{\Phi}(\boldsymbol{X}) = \boldsymbol{0}$ represent the equilibrium conditions.

Boundary conditions. Different boundary conditions can be enforced on the RVEs to retrieve the macro-scale properties [2]. It has been shown that *periodic* boundary conditions (PBCs) provide faster convergence to the effective properties with respect to displacement or traction boundary conditions [10]. Considering the couples of opposite *master* and *slave* external faces of the RVE, the PBCs are enforced as

$$u_i(\boldsymbol{x}^s) = u_i(\boldsymbol{x}^m) + \bar{\Gamma}_{ij}(x_j^s - x_j^m)\,; \qquad t_i(\boldsymbol{x}^s) + t_i(\boldsymbol{x}^m) = 0 \tag{3}$$

where u_i and t_i are the *i*-th components of the displacement and traction fields, respectively. $\boldsymbol{x}^s = \left\{ x_j^s \right\}$ is a point belonging to the slave face, and $\boldsymbol{x}^m = \left\{ x_j^m \right\}$ is a point belonging to the master face.

Morphology generation.

In this study, the micro-morphologies are generated using the Voronoi tessellation algorithm with the Hardcore Laguerre modification [11]. Two types of morphologies are considered: *non-prismatic* periodic morphologies are employed for homogenization, whereas the micro-cracking evolution is studied using prismatic RVEs. Both morphologies take advantage of the regularization scheme developed by Quey et Al. [8], that iteratively removes the small edges whose length is below a predetermined threshold value. Although the technique leads to slightly distorted and non-planar intergranular faces, the resulting morphologies present a drastically reduced number of small geometrical entities.

Non-prismatic **periodic RVEs.** Although it is not strictly required, the use of geometrically periodic morphologies facilitates the enforcement of PBCs by enabling the conformity of the mesh on opposite homologous external faces. Fritzen et Al. [12] proposed a procedure to obtain periodic prismatic morphologies by *a*) copying the initial distribution of seeds into 26 boxes surrounding the original one, *b*) using the Voronoi partition algorithm on the extended box, and *c*) finally cutting the original box out of

extended one. This cutting procedure however produces generally many small geometrical entities, which then become source of undesired mesh refinement. In this work, a new periodic RVE is proposed. In fact, the geometrical periodicity can also be obtained by repeating steps *a*) and *b*), and, instead of using the cutting planes, retaining in the tessellation only the grains whose seeds fall inside the original domain. This simple technique produces a periodic morphology without the drawback of re-introducing small geometrical entities. Given the same distribution of seeds, Fig.1a shows the prismatic periodic morphology, whereas Fig.1b shows the proposed non-prismatic periodic RVE.

(*a*) (*b*)

Fig. 1: *a*) Periodic morphology as obtained after the cutting process. The grains having a volume less than 10% of the mean grain volume are highlighted. *b*) Periodic morphology obtained considering only the grains whose generating seeds fall within the original domain.

Morphology Meshing.

In the literature, either structured or unstructured meshes have been successfully used for polycrystalline aggregates in FEM [12,13] or BEM [4,5] frameworks. In this work, the discontinuous mesh used in [4] is replaced by a continuous/semi-discontinuous approach that, as it will be shown later, leads to a remarkable reduction in the overall number of degrees of freedom (DoFs) for the problem in hand without loss of accuracy. The computational saving in terms of DoFs for a sample grain face is clearly shown in Fig.2 where, starting from a given distribution of edge nodes, Fig.2a, and the mesh of the face Fig.2b, the collocation nodes obtained from a discontinuous approach, Fig.2c are compared to those obtained using the proposed approach, combining triangular and quadrangular elements. Finally, Fig.3 shows the comparison between a generic grain meshed using a triangular mesh, and the same grain meshed using the proposed meshing algorithm. It is worth noting that *the robustness of the meshing algorithm is not a trivial issue when dealing with Voronoi tessellations, due to the high statistical variability of their morphological features*.

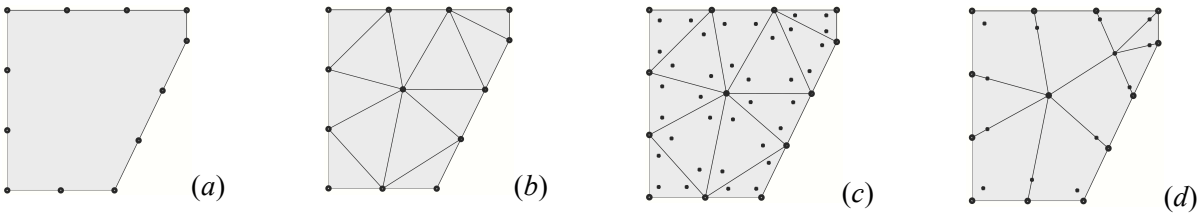

(*a*) (*b*) (*c*) (*d*)

Fig. 2: *a*) Sample face with edge nodes; *b*) 2D face mesh; *c*) Position of the collocation nodes when a discontinuous approach is adopted; *d*) Position of the collocation nodes when the continuous/semi-discontinuous approach is adopted. Big dots represent geometrical nodes; small dots are collocation nodes.

(*a*) (*b*)

Fig. 3: *a*) Surface triangular mesh of a generic grain; *b*) Surface mesh of the same grain using the optimized meshing algorithm with triangular and quadrangular elements.

Computational Tests.

In this section, the homogenization accuracy and the performance of the micro-cracking algorithm are considered.

Overall computational savings. The overall computational savings obtained in the proposed framework are presented and discussed in terms of overall number of DoFs for the polycrystalline problem. Fig.4a shows the number of DoFs associated with three different meshing approaches, namely continuous, discontinuous and continuous/semi-discontinuous. The continuous mesh is shown only for comparison purposed but it was not considered in the analyses as it introduces complexities in the formulation in terms of corner nodes at the edges of the grains. From Fig.4a, it can be noted that there are remarkable savings in terms of number of DoFs between the discontinuous and the proposed approach. It can also be noted that the Voronoi regularization scheme contributes on the overall savings. On the other hand, Fig.4b shows how the use of non-prismatic RVEs allow to further reduce the overall number of DoFs.

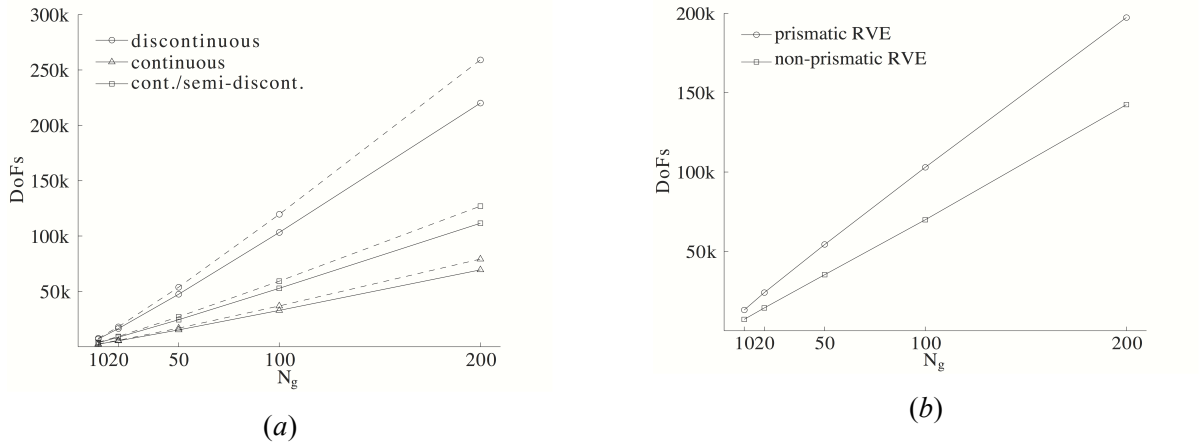

Fig 4: *a*) Comparison between the number of DoFs vs N_g obtained using the discontinuous and the continuous/semi-discontinuous approach. The number of DoFs considering a continuous 2D mesh are also reported for reference purposes. The dashed lines refer to non-regularized morphologies; the solid lines to regularized morphologies. *b*) Comparison between the number of DoFs vs N_g obtained using prismatic and non-prismatic RVEs. In *a*-*b*) data was collected over 100 realizations for each N_g considered.

Computational homogenization. In this section, the developed model is employed to determine the effective properties of polycrystalline aggregates using the non-prismatic periodic RVEs and the PBCs presented above. In this study, two materials are considered, namely crystalline copper and a two-phase steel. For both materials, aggregates with $N_g = \{10, 20, 50, 100, 200\}$ are tested. The homogenization results are then presented in terms of apparent Young's modulus as ensemble averages obtained over 100 realizations.

Fig.5a shows the apparent Young's modulus versus the number of grains N_g calculated using kinematic boundary and periodic boundary conditions. As expected, when PBCs are used, the averaged property approaches much faster the macroscopic property with respect to the case of kinematic boundary conditions. Fig.5b presents the apparent Young's modulus of the two-phase SAF 2507 stainless steel, and of its two constituents, namely α-Iron (42% in volume) and γ-Iron (58% in volume). As it can be seen, the apparent property approaches the known value of the alloy. The slight misalignment of the curves has been added for the sake of clarity. It is worth noting that, considering 200-grain morphologies, the apparent properties approach the effective ones within a 1.50% error.

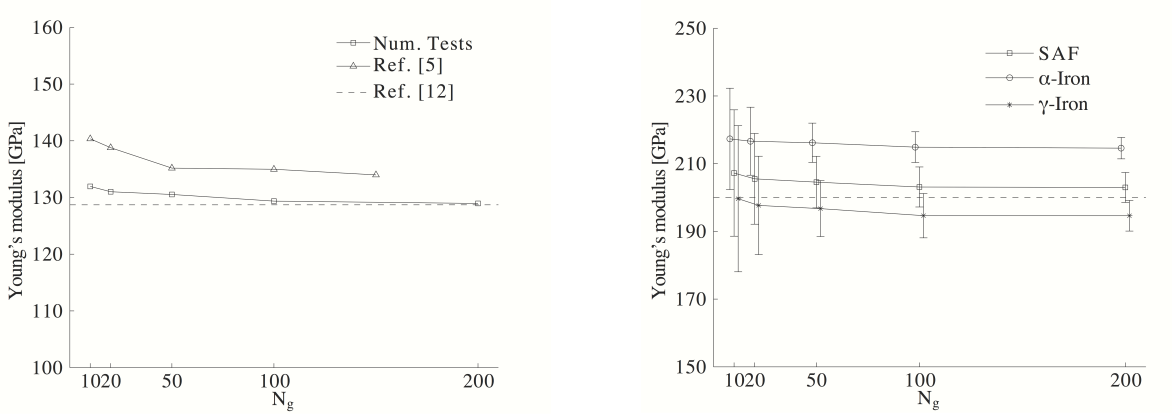

(*a*) (*b*)

Fig. 5: Apparent Young's moduli for *a*) polycrystalline copper, and for *b*) two-phase stainless steel SAF 2507 and its constituents.

Micro-cracking tests. In this section, a few micro-cracking tests are reported in order to test the performance of the developed model in terms of solution time of the non-linear micro-cracking simulations. The simulations are performed considering SiC aggregates whose bulk crystal constants and interface frictional-cohesive law parameters are taken from Ref. [5]. The micro-cracking simulations are performed on prismatic morphologies using non-periodic kinematic boundary conditions, since the use of PBCs on non-prismatic RVEs require some special considerations that are currently being implemented.

Fig.6 shows the micro-cracking tests performed on 100-grain aggregates with different values of the ASTM grain size $G = 10, 12, 14$ under tensile load in displacement control. Fig.6a reports the volume averaged macro stress Σ_{33} versus the nominal strain. It is worth noting that significantly different macro-behaviours in terms of brittleness correspond to different ASTM grain sizes: aggregates with bigger grains (ASTM $G = 10$) are more brittle than those with smaller grains; this is consistent with the model physics.

Fig.7 shows instead the same analysis performed on morphologies with the same ASTM grain size $G = 12$, but with different number of grains $N_g = 50, 100, 200$. In this case, it is interesting to note that the tests with $N_g = 100$ and $N_g = 200$ show similar macro-behaviour, so that it appears reasonable to assume the existence of a representative volume.

In conclusion, it may be of interest to mention that the use of regularized morphologies and optimized meshes reduce the solution time of micro-cracking analyses from several *days* to several *hours*.

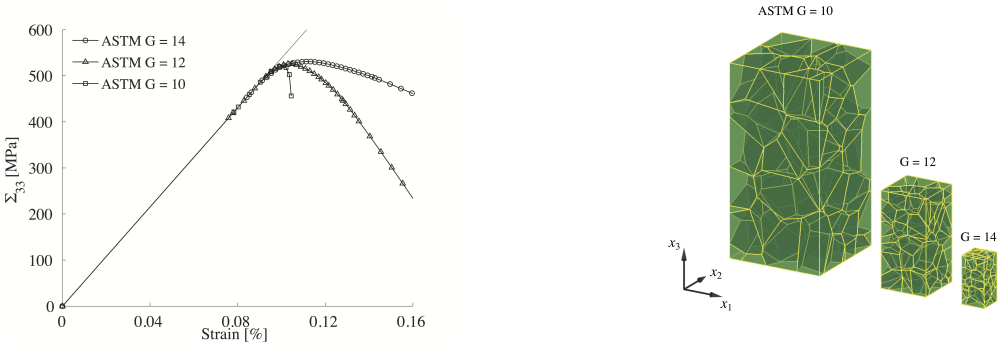

(*a*) (*b*)

Fig. 6: *a*) Volume averaged stress component Σ_{33} versus nominal applied strain Γ_{33}; *b*) Relative size of three different morphologies with $N_g = 100$ and different ASTM grain size $G = 10, 12, 14$.

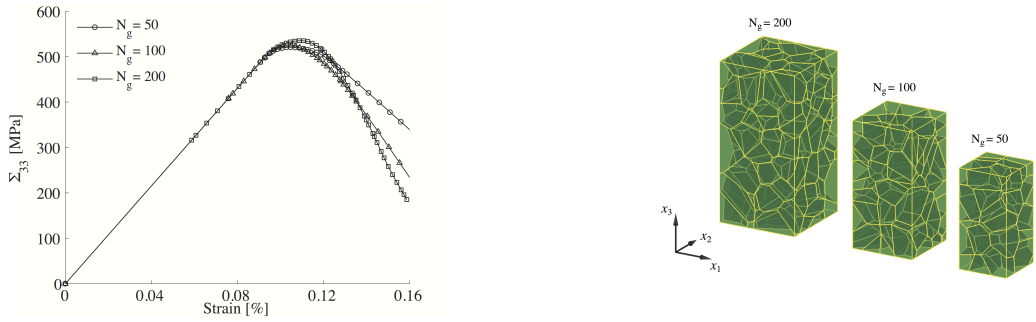

(*a*) (*b*)

Fig. 7:*a*) Volume averaged stress component Σ_{33} versus nominal applied strain Γ_{33} for the *b*) morphologies with ASTM grain size $G = 12$ and $N_g = 50,\ 100,\ 200$.

Acknowledgements

The authors gratefully acknowledge the technical support from the Staff of the Italian Centre for Super Computing Applications and Innovation (SCAI) of CINECA, for the use of their HPC infrastructure.

References

[1] EB Tadmor, RE Miller. *Modeling Materials: continuum, atomistic and multiscale techniques*, Cambridge University Press, **2011**
[2] T Kanit, S Forest, I Galliet, V Mounoury, D Jeulin, *International Journal of Solids & Structures*, **40**, 3647-3679, **2003**
[3] I Simonovski, L Cizelj, Grain-scale modeling approaches for polycrystalline aggregates, in Polycrystalline Materials — Theoretical and Practical Aspects, Z Zakhariev (ed), Vol. 125, InTech, Oxford, pp. 49–74, 2012
[4] I Benedetti, MH Aliabadi. *Computational Materials Science*, **67**, 249-260, **2013**
[5] I Benedetti, MH Aliabadi. *Computer Methods in Applied Mechanics and Engineering*, **265**, 36-62, **2013**
[6] I Benedetti, F Barbe. Modelling Polycrystalline Materials: An overview of three-dimensional grain-scale mechanical models. *Journal of Multiscale Modelling*, *5*(01), **2013**
[7] I Benedetti, MH Aliabadi. *Computer Methods in Applied Mechanics and Engineering*, **289**, 429-453, **2015**
[8] R Quey, PR Dawson and F Barbe, *Computer Methods in Applied Mechanics and Engineering*, **200**, 1729-1745, **2011**
[9] MH Aliabadi, *The boundary element method: applications in solids and structures*, Wiley, **2002**
[10] K Terada, M Hori, T Kyoya, N Kikuchi, *Int Journal of Solids & Structures*, **37**, 2285-2311, **2000**
[11] Z Fan, Y Wu, X Zhao, Y Lu, *Computational Material Science*, **29**, 301-308, **2004**
[12] F. Fritzen, T. Böhlke, E. Schnack, *Computational Mechanics*, **43**, 701-713, **2009**
[13] T. Böhlke, K. Jöchen, O. Kraft, D. Löhe, V. Schulze, *Mechanics of Materials*, **42**, 11-23, **2010**